# A New Apparatus for Coupled Low-field NMR And Ultrasonic Measurements in Rocks at Reservoir Conditions

*Paul R. J.* Connolly[1], *Joël* Sarout[2], *Jérémie* Dautriat[2], *Eric F.* May[1], *Michael L.* Johns[1]

[1]Department of Chemical Engineering, M050, The University of Western Australia, 35 Stirling Highway, CRAWLEY WA 6009, Australia.

[2]CSIRO Energy, ARRC Laboratories Kensington, Perth 6151, WA, Australia.

**Abstract.** Models which describe the effect of pore fluids on elastic wave propagation in rocks are the basis for quantitative reservoir analysis. Laboratory ultrasonic measurements conducted on rock cores are often used to test the applicability of the various models and adapt them as required. Current saturation-wave velocity models usually require some description of fluid saturation and/or distribution, pore aspect ratio, wettability and fluid viscosity. These are often measured indirectly at different experimental conditions to the reservoir or simply assumed. Hydrogen ($^1$H) Nuclear magnetic resonance (NMR) is a technique that can be used to quantitatively describe some of these important parameters. Here we report the design and performance of a novel NMR-compatible core holder system allowing for the measurement of both ultrasonic P-wave velocities and NMR relaxation parameters in rock cores at reservoir pressure and at variable fluid saturation conditions. Successful validation against a conventional benchtop ultrasonic measurement system was performed using a dry Berea sandstone core, whilst sequential NMR and ultrasonic measurements were performed on a Bentheimer Sandstone core at reservoir pressures and as a function of variable brine saturation (core flooding conditions). To the authors' knowledge, this new apparatus represents the first documented example of coupled high temperature NMR and ultrasonic measurements conducted at the same experimental conditions on the same rock specimen, and allows for a new approach to study pore scale saturation effects on elastic wave propagation in rocks.

## 1 Introduction

Low field Hydrogen ($^1$H) Nuclear Magnetic Resonance (NMR) is an important tool in petrophysics and is readily used to determine important reservoir parameters such as porosity, permeability, fluid type and saturation. Measurements are made both *in situ* in reservoirs using well logging tools, and *ex situ* on recovered reservoir plugs using benchtop spectrometers [1]. For quantitative assessment, low-field NMR employing magnetic field strengths less than 0.5 T have been shown to be more robust than higher fields as the impacts of internal magnetic field gradients are minimized [2], [3]. Furthermore, due to the technological challenge of operating well logging tools on long wire lines in harsh reservoir conditions, only low magnetic fields (e.g. ~<0.1T) are currently attainable [4].

Another key toolbox used in quantitative reservoir assessment and dynamic reservoir monitoring is seismic attribute analysis. The propagation of elastic waves in rocks can be related to their key lithological and geomechanical properties [5], and is also sensitive to the properties of the pore fluids [6]. Regional scale seismic surveys are used to map subsurface structures and delineate economic concentrations of hydrocarbons [7]. Furthermore, with improvements in 4D seismic techniques, effective monitoring of reservoir fluids during hydrocarbon production [8], [9] and $CO_2$ sequestration [10], [11] has been demonstrated. The interpretation of seismic data requires seismic inversion, which is generally constrained by rock physics models based on calibrated laboratory measurements. These rock physics models relate the elastic properties of rocks to effective stress, rock anisotropy, lithological and geomechanical properties, and also consider the impact of pore fluids (e.g. [5], [12]–[14]). A critical aspect in the application of these models to seismic reservoir characterisation and time lapse monitoring is their ability to predict the elastic response of rocks partially saturated with multiple pore fluids.

* Corresponding author: paul.connolly@uwa.edu.au

By combining laboratory ultrasonic and NMR measurements to directly quantify important parameters like wettability, pore surface-to-volume ratios and saturation, we aim to provide new insight on elastic wave propagation in saturated and partially saturated rocks. Furthermore, the ability to calibrate these measurements directly against *in situ* reservoir ultrasonic and NMR measurements made by wireline logging tools may also offer a novel approach to improving well log interpretation. Here, we present, as far as the authors are aware, the first example of an NMR compatible core flooding system capable of measuring ultrasonic wave velocities at high temperature and pressure conditions. The system has been designed to fit within the constraints of a 53mm borehole which is typical for low field NMR instruments used for rock core analysis. Only one other example of combined NMR and ultrasonic measurements of geological material was cited in the literature where the authors utilised a small animal Magnetic Resonance Imaging (MRI) system (85.7 MHz $^1$H or 2.0 T magnet) to study the formation of methane hydrates in sand packs. We have conducted a series of preliminary tests in a 2 MHz $^1$H NMR spectrometer up to temperatures and pressures of 45°C and 21 MPa. The design challenges and noise considerations are discussed, comparisons to a well-established ultrasonic measurement standard are made, and initial results are reported for a dry Berea sandstone and for a Bentheimer sandstone saturated with variable amounts of brine and supercritical $CO_2$.

## 2 Materials and Methods

### 2.1 Rock samples

Two quartz-dominated sandstone rock cores widely considered as petro-physical standards, Berea and Bentheimer, were used in this study. For comparison purposes, ultrasonic data on a dry Berea sandstone were acquired with both our novel apparatus and a well-established instrument, namely, the Autonomous Triaxial Cell (ATC) available at the Commonwealth Scientific and Industrial Research Organisation (CSIRO) in Perth, Australia [12]–[15]. The gravimetrically determined porosity for this core sample was 19.4%. The original Berea sandstone core had an original diameter of 3.81 cm and a length of 4.60 cm. The P-wave velocity in this dry core was first measured on a benchtop ultrasonic system. To adapt this core to our new NMR-Ultrasonic core holder (and with the desire to repeat the experiments on the same sample), its diameter was reduced to 2.54 cm using a diamond grinding wheel. For the core flooding tests a Bentheimer core was used due to its lower clay content and well-established NMR response [16], [17]. The core sample used had a diameter of 2.54 cm and was 11.45 cm long, with a gravimetrically-determined porosity of 21% and a permeability (to brine) of 3.4 D.

### 2.2 NMR relaxation time measurements

NMR signal or magnetisation ($\mathbf{M}_{(t)}$) decay occurs via two mechanisms, namely spin-spin ($T_2$) and spin-lattice ($T_1$) relaxation, corresponding to the transverse and longitudinal components of the magnetic field, respectively. Longitudinal recovery is described by:

$$\frac{\mathbf{M}_{(t)}}{\mathbf{M}_{(0)}} = 1 - exp\left\{-\frac{t}{T_1}\right\}, \quad (1)$$

while the transverse component decay is described by:

$$\frac{\mathbf{M}_{(t)}}{\mathbf{M}_{(0)}} = exp\left\{-\frac{t}{T_2}\right\}. \quad (2)$$

Measuring $T_2$ relaxation times can be achieved significantly faster than measuring $T_1$ relaxation times, whilst providing similar pore scale information. Hence $T_2$ times are a standard measurement approach for reservoir rock characterisation. When bound in a porous medium, proton ($^1$H) spins interacting with pore walls undergo enhanced relaxation due to increased dipolar interactions and/or restrictions to molecular mobility. Brownstein and Tarr [18] showed that for a fluid contained in a restricted environment, $T_2$ measured using a CPMG sequence can be modelled as:

$$\frac{1}{T_2} = \frac{1}{T_{2,bulk}} + \rho_s \frac{S}{V} + D_0 \frac{(\gamma G t_e)^2}{12}, \quad (3)$$

where $S/V$ is the surface-to-volume ratio of the pores; $\rho_s$ is the surface relaxivity constant representing the magnitude of proton ($^1$H) relaxation enhancement from surface interactions; $D_0$ is the fluid's self-diffusion coefficient; $\gamma$ is the gyromagnetic ratio of a proton nuclei; $G$ is any magnetic field gradients (in fluid-saturated rocks these are induced by the difference in magnetic susceptibility between phases); and $t_e$ is the time between NMR spin echoes. Typically, the impact of diffusive decay is negligible for conventional porous sandstones analysed with low magnetic field instruments (such as the 0.049 T system used here) and where sufficiently short echo times are used [19].

Considering $T_2$ times as a proxy for fluid-filled pore sizes is well-established [20]. This correlation assumes that diffusive exchange between pores is slow compared to the timescale of a measurement. For heterogeneous porous materials such as rocks, the observed $T_2$ response is represented by a convolution of exponentially decaying signals arising from pores of different sizes:

$$\frac{\mathbf{M}_{(t)}}{\mathbf{M}_{(0)}} = \frac{1}{V_0}\sum_{i}^{n}\left(V_i \times \left(e^{-t/T_{2,i}}\right)\right), \quad (4)$$

where $V_0$ and $V_i$ are the total sample volume and the $i^{th}$ pore volume contribution respectively; $n$ is the number of pores; $\mathbf{M}_{(0)}$ is the equilibrium magnetisation; and $T_{2,i}$ is the relaxation rate for the $i^{th}$ pore [21]. To solve for the probability distribution of relaxation times the raw NMR data must be inverted. Tikhonov's regularisation [22] is

well suited to this ill-posed problem and has been used here. This method differs from a simple minimisation of residual norms in that an additional penalty term is added to balance the impact of noise. A more detailed description of Tikhonov's regularisation, as implemented here, can be found in Connolly *et al.* [23].

All NMR measurements presented here were made using a Magritek (New Zealand) Rock Core Analyzer (RCA) with a magnetic field strength of 0.049 T (corresponding to a $^1$H Larmor frequency of 2 MHz) and a 54 mm r.f. probe with a minimum echo time of 100 µs. To demonstrate the combination of NMR and ultrasonic velocity measurements on a sample at reservoir conditions, NMR transverse ($T_2$) relaxation time measurements were made on a Bentheimer sandstone core after sequential injection of brine and supercritical carbon dioxide. The calibrated NMR signal amplitude determines the brine filled porosity and the $T_2$ times are indicative of the pore sizes the brine occupies [4], [22]. All $T_2$ relaxation time measurements were made using a standard CPMG pulse sequence [24 - 25].

### 2.3 Ultrasonic pulse transmission measurements

The velocity of the primary compression ($V_P$) and secondary shear ($V_S$) waves in a homogeneous, isotropic and elastic medium are related to its elastic moduli through [5],

$$V_P = \sqrt{\frac{K + \frac{4}{3}\mu}{\rho_m}}, \tag{5}$$

$$V_S = \sqrt{\frac{\mu}{\rho_m}}, \tag{6}$$

where $K$ and $\mu$ stand for the bulk and shear moduli, respectively; and $\rho$ is density.

Here we apply one of the most widely applied methods to measure wave velocities in rocks, the pulse transmission technique where travel times of a single-pulse wave are measured over a known length [26]. In the physics of wave propagation, velocities can be referred to as the phase or group (or energy, or ray) velocity. For the majority of laboratory apparatuses described in the literature, including our new apparatus, the phase velocity is estimated from pulse travel time measurements conducted along the axis of a cylindrical rock specimen. Only in cases for which substantial rock anisotropy exists and/or very small sensor widths (<2mm) are used, can the pulse travel times yield a group velocity [27].

In practice, one transducer is used as the source of mechanical vibration while an opposing transducer is the sensor that converts the propagated mechanical energy back into an electrical signal. Our design utilized ring shaped piezo-ceramics that were nominally P-wave type (polarised along the ring's symmetry axis, which corresponds to the propagation direction) and produce clear first arrival times. These P-wave piezo-ceramics also generate some shear energy, although they are not designed for that purpose. Hence, shear wave arrival times were not determined from our data. Using dedicated shear wave piezo-ceramics allowing for an unambiguous determination of the shear wave velocity is possible and will be a focus for future apparatus development.

Electrical excitation of the source transducer was made using square wave pulses generated by an Olympus 5077PR pulse generator, which can generate pulses up to 400 V at frequencies from 0.1 to 20 MHz. Resulting waveform signals generated at the sensing transducer were captured using an oscilloscope and averaged (stacked) 128 times at a pulse rate of 100 Hz to enhance the signal to noise ratio (SNR). Due to the compliant nature and acoustic impedance compatibility of the PEEK spacers, no additional coupling fluid was required in our new apparatus.

## 3 Apparatus Design and Calibration

### 3.1 Core holder

A FCH series Core Labs NMR-compatible core holder was retrofit with custom-designed fluid distribution plugs made of PEEK, incorporating custom-built ring piezo-ceramics (**Figure 1**). The piezo-ceramic rings and associated electrical connections was designed to ensure the integrity of the fluid distribution plugs. Coaxial cables run through the confining oil ports using Kelmon™ K-25 series high-pressure feed-throughs. A NMR-inert fluorocarbon oil (Fluorinert™ FC-70) was used as the confining medium, and was circulated in the annulus between the primary fluid sealing sleeve and a fluorinated ethylene propylene (FEP) heat shrink sleeve covering the rock core sample. Sealing O-rings made of chemically inert fluroelastomer (Kalrez®) capable of handling corrosive fluids like supercritical $CO_2$ were used. The distribution plugs move freely with an O-ring seal on the injection lines, meaning that at elevated pressure the rock is subject to isotropic stress conditions. The range of operational conditions for the altered design was tested from ambient conditions to a confining pressure of 22 MPa at 45 °C.

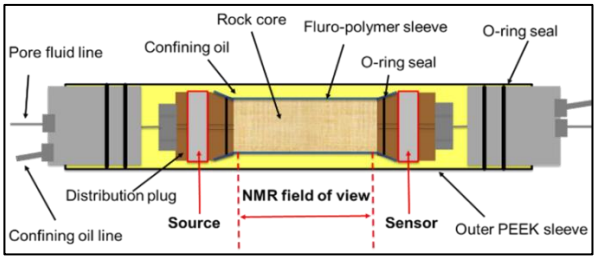

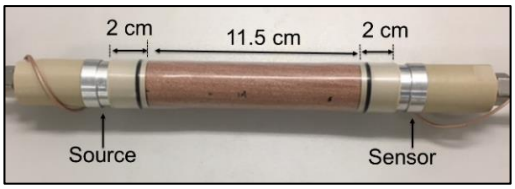


**Figure 1**. Schematic of the assembled core holder (top) and picture of assembled distribution plugs with piezo ceramic source and sensor transducers incorporated (bottom). Sensitive region of the magnet is 10 cm.

Electrically conductive components placed in or near NMR instrumentation usually result in residual eddy currents causing undue electrical noise in the recorded NMR data [28]. Initially, when the assembled core holder was placed inside the magnet borehole residual background noise on the order of 7-8 μV was observed. This level of background noise is approximately two orders of magnitude greater than when the core holder is not present. This noise level is commensurate with the signal typically arising from a fully saturated rock core, making meaningful relaxation time measurements impossible without overly excessive signal averaging. A solution to this problem was obtained by earthing the coaxial lines connected to the ultrasonic transducers, and all metallic components of the core holder and associated injection lines to the base plate of the magnet, effectively reducing the RMS background noise to ~ 0.15 μV, which is only ~ 0.09μV greater than the background RMS noise of an empty system (without core holder). Consequently, the NMR and ultrasonic measurements could be performed sequentially (with a switching time of less than 1 second) with no sample manipulation required ensuring that both measurements were performed at exactly the same stress-pressure-temperature conditions for the respective rock core sample.

Another concern for NMR measurements was the potential distortion of the applied magnetic field ($\mathbf{B_0}$) by having the ultrasonic transducers in or near the homogeneous magnetic field region where the NMR signal is detected (the NMR field of view as shown in the apparatus schematic in **Figure 1**). In the apparatus configuration reported here, the ultrasonic transducers remain on the outer edges of the NMR field of view and did not significantly affect the homogeneity of $\mathbf{B_0}$ within this region (i.e., no change in the full width at half maximum (FWHM) of the NMR spectrum was observed). This was not the case when the transducers were positioned within the NMR field of view, where severe distortions in the $\mathbf{B_0}$ field were observed. Shorter rock cores than used here could be accommodated in this apparatus by simply extending the length of the PEEK distribution plugs, which would ensure that the transducers remained outside the NMR field of view.

### 3.2 Piezo-ceramic Transducers

The characteristic ultrasonic frequencies generated by the piezo-ceramic transducers are defined by their resonant vibrational modes, which are determined by their piezo-elastic and geometric properties. The geometry of the ring-shaped piezo-ceramics used here had dimensions of 19.0 mm OD, 12.0 mm ID and were 2.5 mm thick. The directionally-dependent wave velocities within the piezo-ceramic material as quoted by the manufacturer are 1500, 2040, and 1980 m/s for the planar, axial and radial modes, respectively. The first harmonic vibration modes for flexural motion (in and out of plane bending), and radial and axial contraction were calculated to have frequencies of 104, 429 and 816 kHz, respectively. These ceramics were housed in custom-built aluminium casings while PEEK was used as electrical insulation to shield terminal connections **Figure 2**.

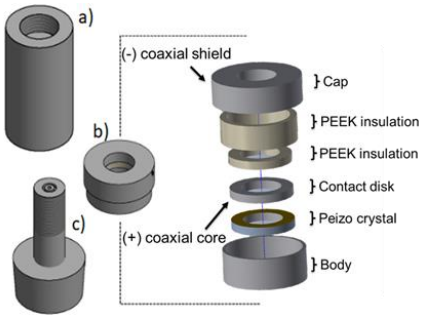


***Figure 2**. a,c) PEEK fluid distribution plugs, b)* custom piezo-ceramic transducer made of aluminium and PEEK. The transducer's electrical contacts rely on mechanical force only (pressure), with the design allowing for PEEK insulation and piezo-ceramic crystals with different dimensions (hence, resonant frequencies) to be interchanged.

The power spectrum of the transducers was measured by placing two transducers in direct contact (face-to-face) and conducting a calibration pulse-transmission test. Single excitation square wave pulses at 400 V with durations of 10, 1 and 0.1 μs at a repetition rate of 100 Hz were used, with the results shown in **Figure 3**. Using piezoelectric charge constants reported by the manufacturer the unconstrained (free) static displacement expected at 400 volts in the axial direction and radial direction are 0.160 μm and 0.029 μm, respectively. The observed frequency response is a convolution of the multiple modes of vibration of the ring-shaped piezo-ceramics (geometry and intrinsic properties), the interface coupling between the piezo-ceramic and the spacer (PEEK), and the body effects of the transducers' casing. Despite this complexity, comparison to the first nodal vibrations the simple calculations mentioned above were reasonable, with peaks at about 80 kHz, a broader band response around 400 kHz and a minor contribution at 830 kHz. When the length of the excitation pulse was increased from 0.1 to 10 μs, the preference for exciting the lower frequency vibrational modes is shown by the increase in the peak at around 80 kHz in **Figure 3**.

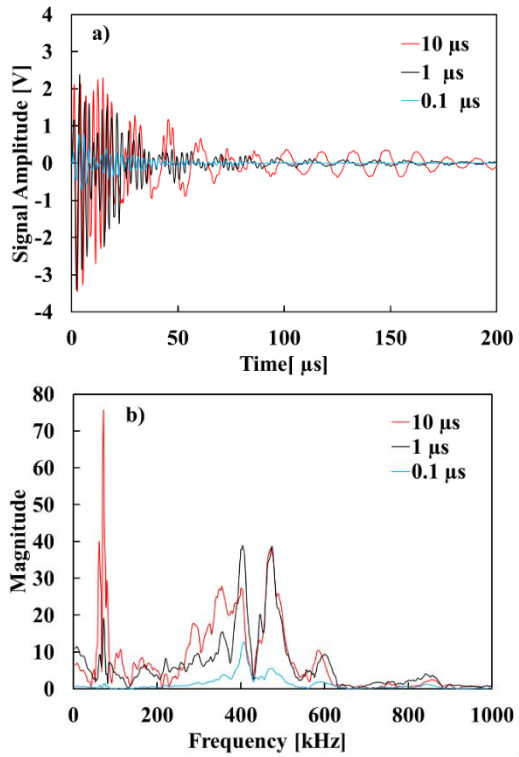


**Figure 3.** a) Time domain signal and b) power spectrum of ring piezo-ceramic transducers in direct contact with one another.

To account for contributions from the PEEK distribution plugs and aluminium casing to the total wave travel times, a calibration of the empty system in which the PEEK distribution plugs were in direct contact (without rock specimen) was conducted. Measurements were taken at temperatures between 25 and 48 °C, and pressures between 1 and 22 MPa. A linear elastic response was observed and fitted with a two-parameter linear model in the form: $ax + by + c$. The resultant fit had a correlation coefficient ($R^2$) of 0.9938 and a Root Mean Square Error (RMSE) of 0.0125 µs. A list of coefficients with corresponding 95% confidence intervals are listed in ***Table 1***. Pressure and temperature inputs to the model were made in Mpa and °C respectively, with the output in µs. Using this calibration mode, the instrument's inherent contribution to the ultrasonic travel times could then be subtracted from measurements carried out on actual rock cores.

***Table 1.*** *Fitting parameters for P-wave PEEK distribution plug time of flight calibration model.*

**Equation: f($p$,$T$)= a$p$ + b$T$ + c**

| Coefficient | Value | 95% confidence bounds | |
|---|---|---|---|
| a | -0.001 | 0.001 | -0.001 |
| b | 0.017 | 0.016 | 0.017 |
| c | 15.8 | 15.78 | 15.82 |

## 4 Results and Discussion

### 4.1 Comparison test

Examples of ultrasonic waveforms acquired with the new NMR-Ultrasonic apparatus in a dry Berea sandstone for increasing confining pressures up to 21 MPa are shown in **Figure 4**. The excitation source was a 400 V 1 µs single-pulsed square wave with a pulse repetition rate of 100 Hz. The SNR of the initial peak amplitude was greater than 1000.

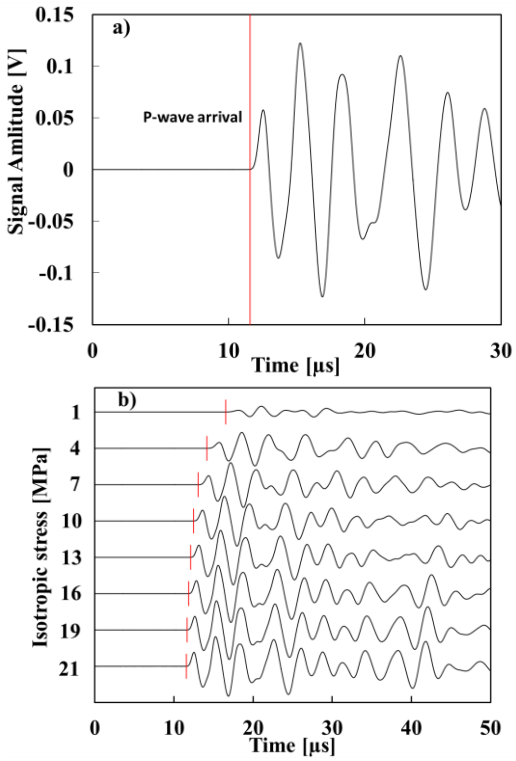


**Figure 4.** a) example of P-wave arrival time and b) response as a function of increasing effective stress. Clear P-wave arrivals are observed with excellent signal-to-noise ratio. Each waveform is typically the average of 128 repeated pulse-transmissions tests at a given pressure condition.

To evaluate the accuracy of P-wave velocities recorded in this new NMR-Ultrasonic apparatus, we conducted comparison measurements on the same rock sample using a well-established Autonomous Triaxial Cell (ATC)[12]–[15]. P-wave velocities were measured at 25°C with a stepwise increase in the confining pressure (3 MPa increments) up to 21 MPa, with repeated measurements at the same confining pressures during unloading. The results of the comparison are shown in **Figure 5** and agree remarkably well for both the loading and the unloading parts of the applied pressure cycle. Increasing wave velocity in rocks with increasing pressure is expected [5] and relates to the compaction of compliant porosity, grain boundaries and matrix defects leading to an increase in the stiffness of the rock frame. Note also that some amount of P-wave velocity hysteresis is observed between the loading and unloading parts of the pressure cycle, which is also a well-documented behaviour [5].

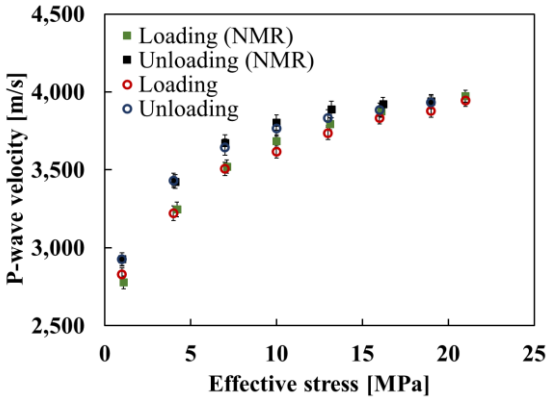


**Figure 5.** Comparison of the P-wave velocity as a function of effective stress for dry Berea sandstone measured using the new NMR-Ultrasonic apparatus (closed squares,) and the well-established Autonomous Triaxial Cell (open circles). The error bars correspond to uncertainties in length and arrival time measurements and typically correspond to ~1% of the estimated P-wave velocity.

### 4.2 Core flooding test

To demonstrate the combined application of NMR and ultrasonic measurements using the new apparatus, a series of core flooding tests involving supercritical $CO_2$ and brine were conducted on the Bentheimer sandstone rock core. The core was vacuumed for 12 hours before dead 3 wt% NaCl brine was injected to a pressure of 10 MPa. Following this, 10 pore volumes of 'live' $CO_2$-saturated brine was injected through the core to achieve an initial 100% brine saturated state. Prior to injection, the 'live' brine was exposed to Bentheimer sandstone for 12 hours to chemically equilibrate the solution, minimising the risk of mineral dissolution effects. The temperature of all fluid pumps, vessels and the core holder were maintained at 40 °C throughout the core flooding experiment. Pressure at the outlet of the core was maintained at 10 MPa with a backpressure regulator. A complete description of the core flooding system used can be found in reference [23]. A series of 10 pore volume aliquots of supercritical $CO_2$ were then injected at flow rates ranging between 20 and 40 ml/min resulting in a number of different partial $CO_2$-brine saturation states. Following this step several pore volumes of $CO_2$-saturated brine were injected at 1 ml/min until a stable saturation was reached, with a portion of the pore space occupied by capillary trapped $CO_2$. After each injection aliquot, NMR transverse relaxation ($T_2$) times and ultrasonic P-wave travel time measurements were carried out. The acquisition and processing of the P-wave arrival times followed the same procedure as the effective stress test on the dry Berea sandstone. Changes in brine saturation were calculated from the decrease in NMR signal relative to the fully saturated state.

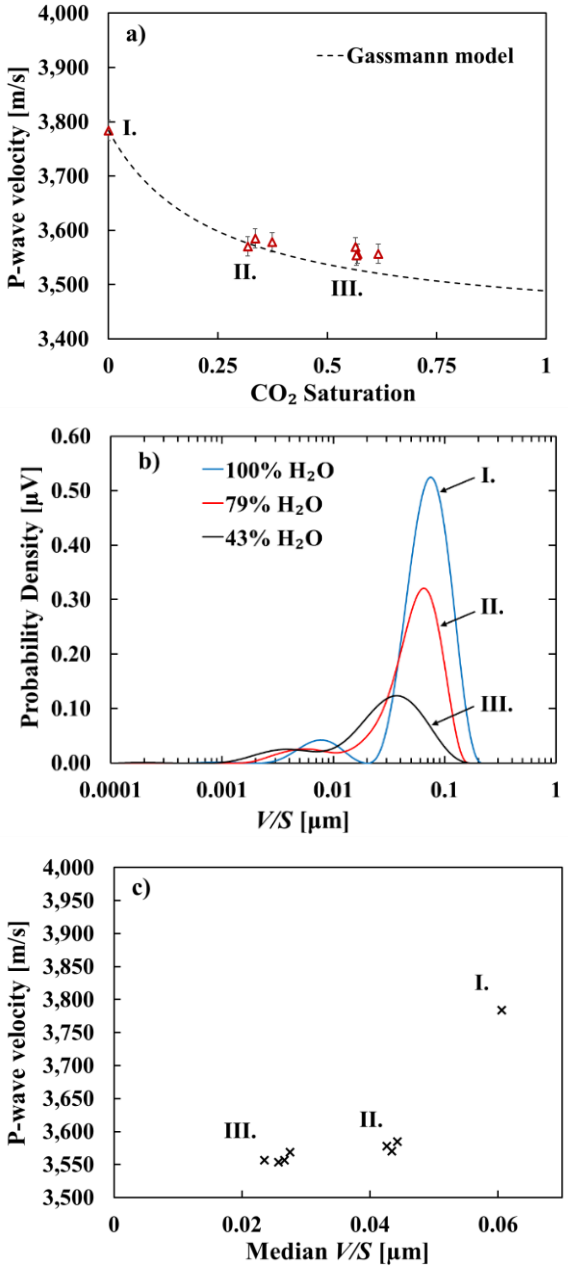


**Figure 6**. a) P-wave velocity in the Bentheimer sandstone at varying levels of supercritical $CO_2$ saturation as determined by NMR signal intensity, b) examples of *V/S* ratio distributions (converted $T_2$ time distributions) of brine-invaded pores at three particular saturation states, i.e., 100%, 79% and 43% brine saturation, and c) corresponding median *V/S* of the brine-invaded pores. Roman numerals indicate data pertaining to saturated (I.), after forced brine imbibition (II.), and after drainage by $CO_{2(sc)}$ injection (III.) respectfully.

**Figure 6** shows the change in P-wave velocity and corresponding change in $T_2$ relaxation times with increasing fraction of supercritical $CO_2$ content. The reduction in $T_2$ relaxation times is direct evidence of pore scale fluid occupation of pores with various surface-to-volume ratios. As the surface relaxivity of Bentheimer sandstone is well-known and quite consistent between

samples, we have converted the $T_2$ times to $V/S$ ratios using a surface relaxivity $\rho_s$ value of 9.5 μm/s [17]. P-wave velocity was observed to decrease with increasing $CO_2$ content as the effective pore fluid compressibility increased. To aid demonstration, we have included the Gassmann's fluid substitution model which remains the most widely used model in the oil & gas industry for predicting P-wave velocity for variable pore fluid compressibility [29], [30]. The largest change in velocity coincides with the preferential displacement of brine from the largest pores, as indicated by the decrease in signal from pores with a larger $V/S$ ratio, and an increase in median relaxation rate ($1/T_2$) (Figure 5). Furthermore, the change in the distributions of $T_2$ times corresponds to the transition between a rock with pores fully saturated with water to one with pores partially occupied by water. Future work will focus on testing NMR determined petro-physical and pore scale saturation properties against the current understanding of how fluid impacts the ultrasonic wave properties in sedimentary rocks.

## 4 Conclusion

A novel design for an NMR compatible rock core holder is presented which allow for the combined measurement of P-wave velocity and NMR fluid responses of rocks at reservoir conditions. The P-wave velocities measured in this system for Berea sandstone at varied effective stress were compared to results from a well-established tri-axial test instrument and showed excellent agreement. Furthermore, pulse transmission velocity measurements of rocks at reservoir conditions are presented for which NMR has been utilised to quantify varied fluid saturation states. This was demonstrated using sequential NMR $T_2$ time relaxation and P-wave velocity measurements on a Bentheimer sandstone that was both fully saturated and partially saturated with brine and supercritical $CO_2$. By converting the $T_2$ times to $V/S$ ratios, these measurements allow for the study of pore fluid effects on elastic wave propagation as a function of fluid occupation in different sized pores. To the author's best knowledge, this is the first example of NMR being used to monitor effects of saturation state whilst recording the P-wave velocity response of a rock at reservoir pressure and temperature conditions. Future work will include extending the application of NMR relaxation, diffusion-weighted and spatially-resolved measurements to further the understanding ultrasonic wave propagation in saturated and partially saturated rocks, and the installation of transversely polarised piezo-ceramic transducers to include the ability to quantitatively determine shear wave velocities.

## 5 References


1. K. Dunn, D. Bergman, and G. LaTorraca, "Chapter 5 NMR logging applications," *Handb. Geophys. Explor. Seism. Explor.*, vol. 32, pp. 129–164, 2002.
2. C. Straley, D. Roosini, H. J. Vinegar, P. Tutunjian, and C. E. Morriss, "Core analysis by low-field NMR," *Log Anal.*, vol. 38, no. April, pp. 84–94, 1997.
3. J. Mitchell, T. C. Chandrasekera, M. L. Johns, L. F. Gladden, and E. J. Fordham, "Nuclear magnetic resonance relaxation and diffusion in the presence of internal gradients: The effect of magnetic field strength," *Phys. Rev. E - Stat. Nonlinear, Soft Matter Phys.*, vol. 81, no. 2, pp. 1–19, 2010.
4. J. Mitchell and E. J. Fordham, "Contributed review: Nuclear magnetic resonance core analysis at 0.3 T," *Rev. Sci. Instrum.*, vol. 85, no. 11, pp. 0–17, 2014.
5. G. Mavko, T. Mukerji, and J. Dvorkin, *The Rock Physics Handbook, Second Edition*. 2009.
6. M. Batzle and Z. Wang, "Seismic properties of pore fluids," *Geophsyics*, vol. 57, pp. 1396–1408, 1992.
7. R. E. Sheriff and L. P. Geldart, *Exploration Seismology*. Cambridge University Press, 1995.
8. R. J. Greaves and T. J. Fulp, "Three-dimensional seismic monitoring of an enhanced oil recovery process," *Geophysics*, vol. 52, no. 09, pp. 1175–1187, 1987.
9. D. Lumley, "Time-lapse seismic reservoir monitoring," *Geophysics*, vol. 66, no. 1, pp. 50–53, 2001.
10. D. Lumley, D. Adams, R. Wright, D. Markus, and S. Cole, "Seismic monitoring of CO2 geosequestration: reaslistic capabilities and limitations," *Annu. Soc. Explor. Geophys. Conf. Expand. Abstr.*, pp. 2841–2845, 2008.
11. R. Arts, A. Chadwick, O. Eiken, S. Thibeau, and S. Nooner, "Ten years' experience of monitoring CO2 injection in the Utsira Sand at Sleipner offshore Norway," *First Break*, vol. 26, no. 1, pp. 65–72, 2008.
12. J. Sarout, C. Delle Piane, D. Nadri, L. Esteban, and D. N. Dewhurst, "A robust experimental determination of Thomsen's δ parameter," *Geophysics*, vol. 80, no. 1, pp. A19–A24, 2015.
13. J. Dautriat, J. Sarout, C. David, D. Bertauld, and R. Macault, "Remote monitoring of the mechanical instability induced by fluid substitution and water weakening in the laboratory," *Phys. Earth Planet. Inter.*, vol. 261, pp. 69–87, 2016.
14. L. Pimienta, L. Esteban, J. Sarout, K. Liu, J. Dautriat, C. Delle Piane, and M. B. Clennell, "Supercritical CO2injection and residence time in fluid-saturated rocks: Evidence for calcite dissolution and effects on rock integrity," *Int. J. Greenh. Gas Control*, vol. 67, no. September, pp. 31–48, 2017.
15. C. Delle Piane and J. Sarout, "Effects of water and supercritical CO2on the mechanical and elastic properties of Berea sandstone," *Int. J. Greenh. Gas Control*, vol. 55, pp. 209–220, 2016.
16. H.-K. Liaw, R. Kulkarni, S. Chen, and a. T. Watson, "Characterization of fluid distributions in porous media by NMR techniques," *AIChE J.*, vol. 42, no. 2, pp. 538–546, 1996.
17. K. E. Washburn, M. Sandor, and Y. Cheng, "Evaluation of sandstone surface relaxivity using laser-induced breakdown spectroscopy," *J. Magn. Reson.*, vol. 275, pp. 80–89, 2017.
18. K. R. Brownstein and C. E. Tarr, "Spin-lattice

relaxation in a system governed by diffusion," *J. Magn. Reson.*, vol. 26, no. 1, pp. 17–24, 1977.
19. J. Mitchell, T. C. Chandrasekera, M. L. Johns, L. F. Gladden, and E. J. Fordham, "Nuclear magnetic resonance relaxation and diffusion in the presence of internal gradients: The effect of magnetic field strength," *Phys. Rev. E*, vol. 81, no. 2, pp. 1–19, 2010.
20. R. L. Kleinberg, "Pore size distributions, pore coupling, and transverse relaxation spectra of porous rocks," *Magn. Reson. Imaging*, vol. 12, no. 2, pp. 271–274, 1994.
21. O. Mohnke and B. Hughes, "Jointly deriving NMR surface relaxivity and pore size distributions by NMR relaxation experiments on partially desaturated rocks," *Water Resour. Res.*, vol. 50, no. 6, pp. 5309–5321, 2014.
22. A. N. Tikhonov, "Solution of Incorrectly Formulated Problems and the Regularisation Method.pdf," *Sov. Math. Dokl.*, vol. 4, no. 4, pp. 1035–1038, 1963.
23. P. R. J. Connolly, S. J. Vogt, S. Iglauer, E. F. May, and M. L. Johns, "Capillary trapping quantification in sandstones using NMR relaxometry," *Water Resour. Res.*, pp. 1–16, 2017.
24. H. Y. Carr and E. M. Purcell, "Effects of diffusion on free precession in nuclear magnetic resonance experiments," *Phys. Rev.*, vol. 94, no. 3, pp. 630–638, 1954.
25. S. Meiboom and D. Gill, "Modified spin-echo method for measuring nuclear relaxation times," *Rev. Sci. Instrum.*, vol. 29, no. 8, pp. 688–691, 1958.
26. F. Birch, "The velocity of compressional waves in rocks to 10 kilobars: Part 1," *J. Geophys. Res.*, vol. 65, no. 4, pp. 1083–1102, 1960.
27. J. Delllinger and L. Vernik, "Do core sample measurements record group or phase velocity?," *SEG Tech. Progr. Expand. Abstr. 1992*, no. May 2009, pp. 662–665, 1992.
28. M. Terpstra, P. M. Andersen, and R. Gruetter, "Localized eddy current compensation using quantitative field mapping.," *J. Magn. Reson.*, vol. 131, no. 1, pp. 139–143, 1998.
29. F. Gassmann, "Über die Elastizität poröser medien.," *Vierteljahrsschrift der Naturforschenden Gesellschaft Zürich*, vol. 96, pp. 1–23, 1951.
30. F. Yan and D. H. Han, "Effect of pore geometry on Gassmann fluid substitution," *Geophys. Prospect.*, vol. 64, no. 6, pp. 1575–1587, 2016.